ISSN 1674-1056
http://cpb.iphy.ac.cn
http://iopscience.iop.org/cpb
中国物理 B
Chinese Physics
中国物理 Chinese Physics B

Giant topological Hall effect of ferromagnetic kagome metal Fe_3Sn_2

Qi Wang(王琦), Qiangwei Yin(殷蔷薇), Hechang Lei(雷和畅)

Citation: Chin. Phys. B . 2020, 29(1): 017101 . **doi:** 10.1088/1674-1056/ab5fbc
Journal homepage: http://cpb.iphy.ac.cn; http://iopscience.iop.org/cpb

What follows is a list of articles you may be interested in

Possible nodeless $s^{\pm}$-wave superconductivity intwisted bilayer graphene

Zhe Liu(刘哲), Yu Li(李宇), Yi-Feng Yang(杨义峰)

Chin. Phys. B . 2019, 28(7): 077103 . **doi:** 10.1088/1674-1056/28/7/077103

Negative differential resistance and quantum oscillations in $FeSb_2$ with embedded antimony

Fangdong Tang(汤方栋), Qianheng Du(杜乾衡), Cedomir Petrovic, Wei Zhang(张威), Mingquan He(何明全), Liyuan Zhang(张立源)

Chin. Phys. B . 2019, 28(3): 037104 . **doi:** 10.1088/1674-1056/28/3/037104

Magnetochemistry and chemical synthesis

Lin Hu(胡林), Guoliang Xia(夏国良), Qianwang Chen(陈乾旺)

Chin. Phys. B . 2019, 28(3): 037102 . **doi:** 10.1088/1674-1056/28/3/037102

Heavy fermions in high magnetic fields

M Smidman, B Shen(沈斌), C Y Guo(郭春煜), L Jiao(焦琳), X Lu(路欣), H Q Yuan(袁辉球)

Chin. Phys. B . 2019, 28(1): 017106 . **doi:** 10.1088/1674-1056/28/1/017106

Pressure effect in the Kondo semimetal $CeRu_4Sn_6$ with nontrivial topology

Jiahao Zhang(张佳浩), Shuai Zhang(张帅), Ziheng Chen(陈子珩), Meng Lv(吕孟), Hengcan Zhao(赵恒灿), Yi-feng Yang(杨义峰), Genfu Chen(陈根富), Peijie Sun(孙培杰)

Chin. Phys. B . 2018, 27(9): 097103 . **doi:** 10.1088/1674-1056/27/9/097103

Giant topological Hall effect of ferromagnetic kagome metal Fe_3Sn_2*

Qi Wang(王琦), Qiangwei Yin(殷蔷薇), and Hechang Lei(雷和畅)†

Department of Physics and Beijing Key Laboratory of Opto-electronic Functional Materials & Micro-nano Devices, Renmin University of China, Beijing 100872, *China*

(Received 22 October 2019; revised manuscript received 23 November 2019; accepted manuscript online 9 December 2019)

We present the experiment observation of a giant topological Hall effect (THE) in a frustrated kagome bilayer magnet Fe_3Sn_2. The negative topologically Hall resistivity appears when the field is below 1.3 T and it increases with increasing temperature up to 300 K. Its maximum absolute value reaches ~ 2.01 μΩ·cm at 300 K and 0.76 T. The origins of the observed giant THE can be attributed to the coexistence of the field-induced skyrmion state and the non-collinear spin configuration, possibly related to the magnetic frustration interaction in Fe_3Sn_2.

Keywords: topological Hall effect, skyrmion state, non-collinear spin configuration

PACS: 71.27.+a, 71.55.Ak, 75.50.–y **DOI:** 10.1088/1674-1056/ab5fbc

1. Introduction

The ordinary Hall effect is due to the Lorentz force acting on the charge carriers.[1] In ferromagnetic materials, an extra contribution arises from spin–orbit coupling, which is proportional to the spontaneous magnetization, termed the anomalous Hall effect (AHE).[2,3] The origins of AHE are separated into intrinsic[4] and extrinsic (skew scattering and side jump) mechanisms.[5–7] The intrinsic mechanism has been attributed to the Berry curvature in momentum space.[8–11] Furthermore, in a non-coplanar spin configuration, the Berry phase arising from the real-space scalar spin chirality $\chi_{ijk} = \boldsymbol{S}_i \cdot (\boldsymbol{S}_j \times \boldsymbol{S}_k)$ can generate a fictitious magnetic field and hence give rise to the topological Hall effect (THE).[12,13] It is widely known that THE is commonly observed in metallic magnets hosting magnetic skyrmions, which are topologically protected whirling spin textures in nanoscale.[14] The noncentrosymmetric B20 magnets with skyrmions, such as MnSi,[15–17] MnGe,[18] FeGe,[19,20] and $Mn_{1-x}Fe_xSi$,[21] as well as centrosymmetric magnets MnNiGa[22] and MnPdGa[23] with biskyrmions are identified to exhibit THE.

Recently, the THE has been observed in frustrated magnetic systems, such as $Pr_2Ir_2O_7$ and $Nd_2Mo_2O_7$ with pyrochlore structure,[24,25] $PdCrO_2$, $Fe_{1.3}Sb$, Fe_3GeTe_2, and Gd_2PdSi_3 with triangular lattice,[26–29] Mn_3Sn and Mn_3Ga with kagome lattice,[30,31] and Mn_5Si_3 with noncollinear spin structure.[32] The THE in these systems has attracted much attention. Especially for frustrated centrosymmetric triangular lattice magnet Gd_2PdSi_3, it shows large THE due to the field induced skyrmion lattice. Meanwhile, the magnetic skyrmions in the frustrated centrosymmetric magnetic system have also been studied theoretically.[33–36] These experimental and theoretical results suggest that the magnetic skyrmions can also be stabilized in a centrosymmetric lattice via magnetic frustration without Dzyaloshinskii–Moriya (DM) interaction. Hence geometrically frustrated magnets are also an important material system for the generation of magnetic skyrmions. More importantly, the coexistence of skyrmion state and non-collinear magnetic structure both of which originate from magnetic frustration could result in giant THE.

Frustrated kagome lattice ferromagnet Fe_3Sn_2 has attracted much attention in recent years. It shows a large AHE at temperature below Curie temperature T_C (641 K).[37,38] Moreover, angle resolved photoemission spectroscopy (ARPES) studies confirm the existence of the massive Dirac fermions and flat band.[38,39] Lorentz transmission electron microscopy (LTEM) studies observe skyrmionic bubbles in Fe_3Sn_2 in a wide temperature range above 100 K.[40,41] It is also found that the Fe moments rotate from the *c* axis to the *ab* plane with non-collinear magnetic structures.[42] Stimulated by the above results, in this work, we further investigate the THE of Fe_3Sn_2 in detail. There is a giant topological Hall response in the low-field region and the maximum topological Hall resistivity is about -2.01 μΩ·cm at 300 K and 0.76 T. At high field, the THE disappears due to the fully polarized Fe moments. The giant THE can be related to the field-induced skyrmion structure and the non-collinear spin configuration.

2. Experimental details

Fe_3Sn_2 single crystals were grown by the Fe flux method.[37] The x-ray diffraction (XRD) of a single crystal was performed using a Bruker D8 x-ray machine with Cu K_α radiation. Magnetization and electrical transport mea-

*Project supported by the National Key R&D Program of China (Grant No. 2016YFA0300504), the National Natural Science Foundation of China (Grant Nos. 11574394, 11774423, and 11822412), the Fundamental Research Funds for the Central Universities of China, and the Research Funds of Renmin University of China (RUC) (Grant Nos. 15XNLQ07, 18XNLG14, and 19XNLG17).

†Corresponding author. E-mail: hlei@ruc.edu.cn

© 2020 Chinese Physical Society and IOP Publishing Ltd

surements were carried out in Quantum Design MPMS3 and PPMS-14T, respectively. The longitudinal and Hall electrical resistivities were measured using a four-probe configuration.

3. Results and discussion

The crystal structure of Fe_3Sn_2 is presented in Fig. 1(a), where the Fe–Sn bilayer and Sn layer stack along the c axis alternatively. In an Fe–Sn monolayer, the Fe atoms form a kagome lattice, with the Sn atoms sitting at the centers of the hexagons of the Fe atoms. The Fe–Sn bilayer is composed of two Fe–Sn monolayers shifting from each other by $\boldsymbol{r} = \boldsymbol{a}/3 - \boldsymbol{b}/3 - \boldsymbol{c}/8$. Then, a graphene-like Sn layer is located between two Fe–Sn bilayers. Figure 1(b) shows the longitudinal resistivity $\rho_{xx}(T)$ as a function of temperature at zero field, clearly indicating the metallic behavior of Fe_3Sn_2.

Figure 2(a) shows the magnetic induction B dependence of magnetization $M(B)$ for the Fe_3Sn_2 single crystal at various temperatures with the field along the c axis. The B is calculated by using formula $B = \mu_0(H_{\rm eff} + M) = \mu_0(H + (1 - N_{\rm d})M)$, where $\mu_0 H_{\rm eff}$ is the effective magnetic field, and $N_{\rm d}$ (~ 0.4) is the demagnetizing factor. When the temperature is far below ferromagnetic transition temperature $T_{\rm C}$ (~ 641 K),[37] magnetization $M(B)$ curve of Fe_3Sn_2 increases significantly at the low-field region and then saturates above 1 T because of the complete alignment of Fe moments along the field direction. Moreover, the saturation magnetization $M_{\rm s}$ increases gradually with decreasing temperature, a typical behavior of ferromagnet due to the suppressed excitation of spin waves. Furthermore, the $M_{\rm s}$ at 5 K is about 2.19 $\mu_{\rm B}$/Fe for $B \| c$, well consistent with the values reported in the literature.[37,42–45]

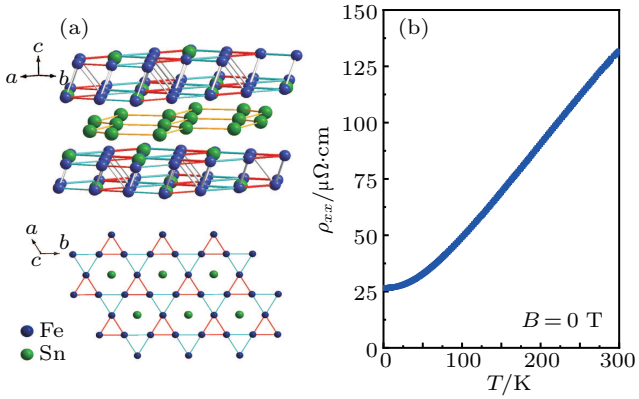


Fig. 1. (a) Crystal structure of Fe_3Sn_2 and top view of one Fe–Sn kagome layer. (b) Temperature dependence of $\rho_{xx}(T)$ at zero field.

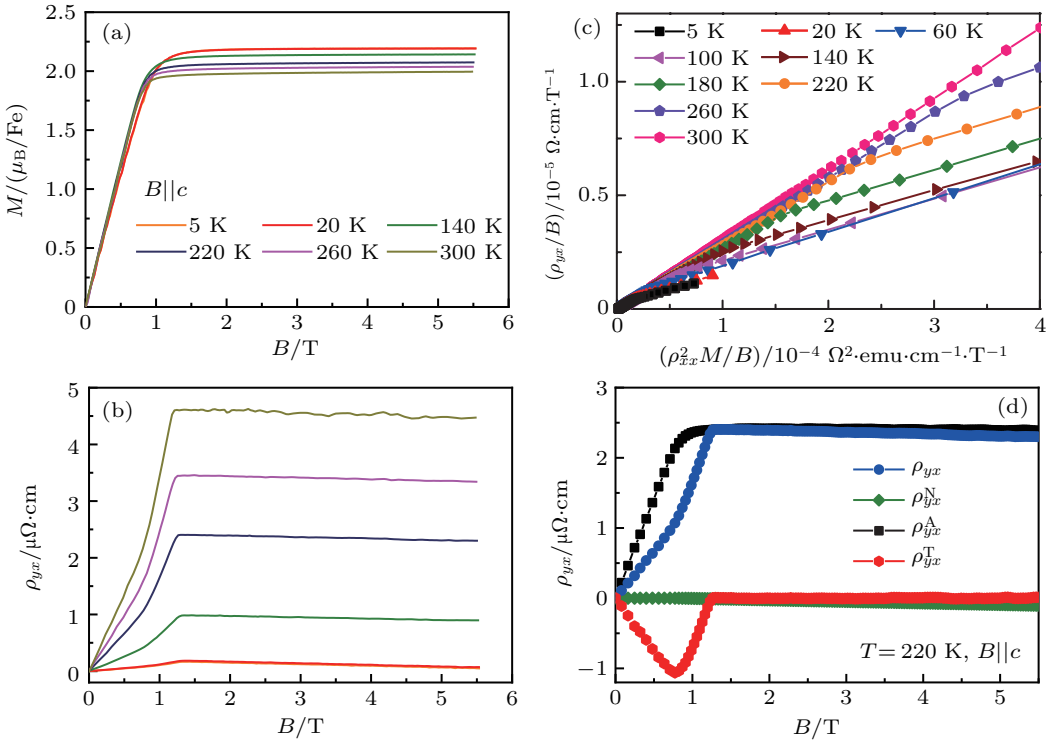


Fig. 2. (a) Magnetization $M(B)$ as a function of magnetic field B at various temperatures with $B \| c$. (b) Field dependence of Hall resistivity $\rho_{yx}(B)$ at various temperatures. The color code is the same as in (a). (c) The relationship between ρ_{yx}/B and $\rho_{xx}^2 M/B$ at various temperatures. (d) Field dependence of different components of the Hall resistivity at 220 K. The blue, green, black, and red lines represent the measured $\rho_{yx}(B)$, $\rho_{yx}^{\rm N}(B)$, $\rho_{yx}^{\rm A}(B)$, and $\rho_{yx}^{\rm T}(B)$, respectively.

Figure 2(b) presents the B-field dependence of Hall resistivity $\rho_{yx}(B)$ at various temperatures when the field is applied parallel to the c axis. The $\rho_{yx}(B)$ curves share similar shape features with $M(B)$, however, there is a key difference between the slopes of the $M(B)$ and $\rho_{yx}(B)$ curves at the low-field region, implying that there might be a THE contribution to $\rho_{yx}(B)$. Above the saturated field, the $\rho_{yx}(B)$ is a linear function of B and decreases slightly, indicating that the domi-

nant carriers in Fe_3Sn_2 are electron-type. As the temperature increases, the saturated value of $\rho_{yx}(B)$ increases and these saturated values at each temperature are well consistent with those in the previous work.[37]

To analysis the THE in Fe_3Sn_2 at the low-field region, the Hall resistivity ρ_{yx} can be expressed as the sum of three different contributions[14,46]

$$\rho_{yx} = \rho_{yx}^{\mathrm{N}} + \rho_{yx}^{\mathrm{A}} + \rho_{yx}^{\mathrm{T}} = R_0 B + S_{\mathrm{H}} \rho_{xx}^2 M + \rho_{yx}^{\mathrm{T}}, \qquad (1)$$

where the first term ρ_{yx}^{N} ($= R_0 B$) is the ordinary Hall resistivity induced by the Lorentz force with the ordinary Hall coefficient R_0, the second term ρ_{yx}^{A} ($= S_{\mathrm{H}} \rho_{xx}^2 M$) is the intrinsic anomalous Hall resistivity and $S_{\mathrm{H}} \rho_{xx}^2$ corresponds to the anomalous Hall coefficient with S_{H} being field independent.[47] The last term ρ_{yx}^{T} represents the topological Hall resistivity arising from scalar spin chirality. When the applied field is strong enough, ρ_{yx}^{T} is supposed to be zero due to the disappearance of chiral spin texture. Hence, using the formula $\rho_{yx}/B = R_0 + S_{\mathrm{H}} \rho_{xx}^2 M/B$, the R_0 and S_{H} can be determined from the y-axis intercept and slope of the linear fit of ρ_{yx}/B vs. $\rho_{xx}^2 M/B$ curve in the high-field region, as shown in Fig. 2(c). Here, the fitting range is between 1.4 T and 5.5 T, below this region the curves deviate from linearity, implying the emergence of THE. The R_0 determined from this scaling is negative at various temperatures, confirming that the electron-type carrier is dominant in Fe_3Sn_2. The magnitude of R_0 is about 1×10^{-8} $\Omega\cdot\mathrm{cm}\cdot\mathrm{T}^{-1}$, well consistent with the reported value.[37] The S_{H} is almost a constant (~ 0.033–0.039 V^{-1}) and it turns out that the intrinsic mechanism makes a dominant contribution to the anomalous Hall resistivity for all temperatures at high field.[47]

Then the values of ρ_{yx}^{T} can be obtained by extracting the calculated ρ_{yx}^{N} and ρ_{yx}^{A} from the total ρ_{yx}. As shown in Fig. 2(d), at a selected temperature $T = 220$ K, $\rho_{yx}^{\mathrm{N}}(B)$ (green line) and $\rho_{yx}^{\mathrm{A}}(B)$ (black line) are calculated by using the fitted R_0 and S_{H} values. Accordingly, we obtain the field dependence of $\rho_{yx}^{\mathrm{T}}(B)$ (red line). It can be clearly seen that the $\rho_{yx}^{\mathrm{T}}(B)$ curve shows a hump-like shape and the maximum value $\rho_{yx}^{\mathrm{T,max}}$ is -1.06 $\mu\Omega\cdot$cm at 0.77 T (B_{max}), which is taken as the evidence of THE.[15,17] The derived $\rho_{yx}^{\mathrm{T}}(B)$ at various temperatures from 5 K to 300 K is presented in Fig. 3(a). A sizable $\rho_{yx}^{\mathrm{T}}(B)$ can be observed over the whole temperature range and the sign of $\rho_{yx}^{\mathrm{T}}(B)$ is negative at all temperatures. The absolute value of $\rho_{yx}^{\mathrm{T}}(B)$ increases firstly, then goes through a maximum with increasing field. Finally, it disappears when the field is higher than 1.3 T, possibly due to the fully alignment of Fe moments along the field direction. This result is well consistent with the saturated field of the $M(B)$ curve. Although the B_{max} is almost temperature independent (~ 0.8 T), the amplitude of $\rho_{yx}^{\mathrm{T,max}}$ increases monotonically with increasing temperature, as shown in Fig. 3(b). The largest $|\rho_{yx}^{\mathrm{T,max}}|$ (~ 2.01 $\mu\Omega\cdot$cm at $B = 0.76$ T) appears at 300 K, much larger than those of other skyrmion hosting materials such as MnSi (4 n$\Omega\cdot$cm),[15] FeGe (0.16 $\mu\Omega\cdot$cm),[20] and MnNiGa (0.15 $\mu\Omega\cdot$cm).[22]

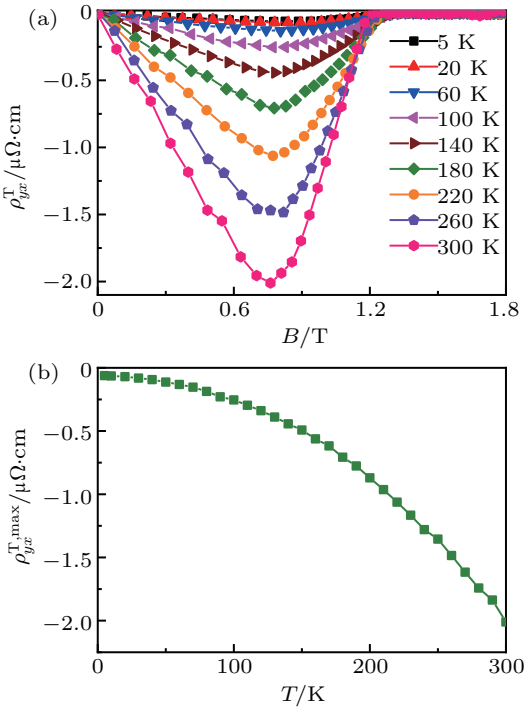


Fig. 3. (a) Magnetic field dependence of $\rho_{yx}^{\mathrm{T}}(B)$ extracted from total Hall resistivity $\rho_{yx}(B)$ at various temperatures. (b) Maximum values of topological Hall resistivity $\rho_{yx}^{\mathrm{T,max}}$ as a function of temperature.

According to the phase diagram of magnetic structure in a previous work,[40] the B_{max} seems to be very close to the boundary area of the transition from magnetic bubbles to skyrmionic bubbles, and the corresponding filed of vanished $\rho_{yx}^{\mathrm{T}}(B)$ is located in the region in which skyrmionic bubbles have disappeared. It seems that the THE might be related to the skyrmion state. If so, in the skyrmion state, the ρ_{yx}^{T} can be written as $\rho_{yx}^{\mathrm{T}} = PR_0B_{\mathrm{eff}}^z$, where P denotes the local spin polarization of the conduction electron, B_{eff}^z is the fictitious effective field, and z is the corresponding direction of the applied field.[15] The polarization P is determined by the ratio between the ordered magnetic moment μ_{spo} in the Skyrmion phase and the saturated moment μ_{sat} taken from the Curie–Weiss moment in the paramagnetic state or the free Fe moment in form of $P = \mu_{\mathrm{spo}}/\mu_{\mathrm{sat}}$.[15] For Fe_3Sn_2, the μ_{spo} at 300 K is 1.764 μ_{B}/Fe at 0.76 T and the μ_{sat} (300 K) is 1.996 μ_{B}/Fe if taken the saturated moment at 5.48 T as an approximate value. Hence, the estimated value of P is 0.88. Taking $R_0 = -4.98(1)\times10^{-4}$ cm^3/C and $\rho_{yx}^{\mathrm{T}} = -2.01$ $\mu\Omega\cdot$cm, the evaluated B_{eff}^z is 45.8 T. In the triangular skyrmion crystal,[40] the emergent magnetic field $B_{\mathrm{eff}}^z = \frac{\sqrt{3}\phi_0}{2\lambda^2}$, where ϕ_0 ($= h/|e| = 4.14\times10^{-15}$ J/A) is the flux quantum for a single electron with h the Planck constant, and λ is the helical period.[14] Hence, the calculated λ is ~ 8.8 nm, much smaller than the periodicity of skyrmionic bubbles (~ 500 nm) at the same field,[40] indicating that the giant THE can not be ascribed solely to the

field-induced skyrmion structure. In addition, the skyrmionic bubble phase only appears above 100 K. But here, the THE can be still observed when the temperature is below 100 K. According to previous results of powder neutron diffraction,[42] there is a spin reorientation transition from the *c* axis to the *ab* plane with decreasing temperature and the moments still do not completely lie in the *ab* plane at 6 K. During this process, it gives rise to a non-collinear spin configuration,[42] possibly leading to a nonzero scalar spin chirality. Thus, both of skyrmion state and non-collinear spin structure will contribute to the extremely large THE in Fe_3Sn_2, especially when $T > 100$ K.

4. Conclusion

In summary, Fe_3Sn_2 shows a giant THE which is observed below 1.3 T at various temperatures. The $|\rho_{yx}^{T}|$ reaches a maximum value ~ 2.01 μΩ·cm at 300 K and 0.76 T. When the field is larger than 1.3 T, the THE disappears as the Fe moments are fully polarized. Detailed analysis suggests that the THE results from the topological magnetic structure in real space. This study will not only deepen our understanding on THE in frustrated magnets, but also help to explore novel frustrated materials with exotic physical properties.

References

[1] Hall E H 1879 *Am. J. Math.* **2** 287
[2] Hall E H 1880 *Philos. Mag.* **10** 301
[3] Hall E H 1881 *Philos. Mag.* **12** 157
[4] Karplus R and Luttinger J M 1954 *Phys. Rev.* **95** 1154
[5] Smit J 1955 *Physica* **21** 877
[6] Smit J 1958 *Physica* **24** 39
[7] Berger L 1970 *Phys. Rev. B* **2** 4559
[8] Jungwirth T, Niu Q and MacDonald A H 2002 *Phys. Rev. Lett.* **88** 207208
[9] Onoda M and Nagaosa N 2003 *Phys. Rev. Lett.* **90** 206601
[10] Haldane F D M 2004 *Phys. Rev. Lett.* **93** 206602
[11] Yao Y G, Kleinman L, MacDonald A H, Sinova J, Jungwirth T, Wang D S, Wang E G and Niu Q 2004 *Phys. Rev. Lett.* **92** 037204
[12] Ye J, Kim Y B, Millis A J, Shraiman B I, Majumdar P and Tešanović Z 1999 *Phys. Rev. Lett.* **83** 3737
[13] Onoda M, Tatara G and Nagaosa N 2004 *J. Phys. Soc. Jpn.* **73** 2624
[14] Nagaosa N and Tokura Y 2013 *Nat. Nanotech.* **8** 899
[15] Neubauer A, Pfleiderer C, Binz B, Rosch A, Ritz R, Niklowitz P G and Böni P 2009 *Phys. Rev. Lett.* **102** 186602
[16] Lee M, Kang W, Onose Y, Tokura Y and Ong N P 2009 *Phys. Rev. Lett.* **102** 186601
[17] Li Y, Kanazawa N, Yu X Z, Tsukazaki A, Kawasaki M, Ichikawa M, Jin X F, Kagawa F and Tokura Y 2013 *Phys. Rev. Lett.* **110** 117202
[18] Kanazawa N, Onose Y, Arima T, Okuyama D, Ohoyama K, Wakimoto S, Kakurai K, Ishiwata S and Tokura Y 2011 *Phys. Rev. Lett.* **106** 156603
[19] Yu X Z, Kanazawa N, Onose Y, Kimoto K, Zhang W Z, Ishiwata S, Matsui Y and Tokura Y 2011 *Nat. Mater.* **10** 106
[20] Huang S X and Chien C L 2012 *Phys. Rev. Lett.* **108** 267201
[21] Yokouchi T, Kanazawa N, Tsukazaki A, Kozuka Y, Kawasaki M, Ichikawa M, Kagawa F and Tokura Y 2014 *Phys. Rev. B* **89** 064416
[22] Wang W H, Zhang Y, Xu G Z, Peng L C, Ding B, Wang Y, Hou Z P, Zhang X M, Li X Y, Liu E K, Wang S G, Cai J W, Wang F W, Li J Q, Hu F X, Wu G H, Shen B G and Zhang X X 2016 *Adv. Mater.* **28** 6887
[23] Xiao X F, Peng L C, Zhao X G, Zhang Y, Dai Y Y, Guo J, Tong M, Li J, Li B, Liu W, Cai J W, Shen B G and Zhang Z D 2019 *Appl. Phys. Lett.* **114** 142404
[24] Machida Y, Nakatsuji S, Maeno Y, Tayama T, Sakakibara T and Onoda S 2007 *Phys. Rev. Lett.* **98** 057203
[25] Taguchi Y, Oohara Y, Yoshizawa H, Nagaosa N and Tokura Y 2001 *Science* **291** 2573
[26] Takatsu H, Yonezawa S, Fujimoto S and Maeno Y 2010 *Phys. Rev. Lett.* **105** 137201
[27] Shiomi Y, Mochizuki M, Kaneko Y and Tokura Y 2012 *Phys. Rev. Lett.* **108** 056601
[28] Wang Y H, Xian C, Wang J, Liu B J, Ling L S, Zhang L, Cao L, Qu Z and Xiong Y M 2017 *Phys. Rev. B* **96** 134428
[29] Kurumaji T, Nakajima T, Hirschberger M, Kikkawa A, Yamasaki Y, Sagayama H, Nakao H, Taguchi Y, Arima T and Tokura Y 2019 *Science* **365** 6456
[30] Rout P K, Madduri P V P, Manna S K and Nayak A K 2019 *Phys. Rev. B* **99** 094430
[31] Liu Z H, Zhang Y J, Liu G D, Ding B, Liu E K, Jafri H M, Hou Z P, Wang W H, Ma X Q and Wu G H 2017 *Sci. Rep.* **7** 515
[32] Sürgers C, Fischer G, Winkel P and Löhneysen H V 2014 *Nat. Commun.* **5** 3400
[33] Okubo T, Chung S and Kawamura H 2012 *Phys. Rev. Lett.* **108** 017206
[34] Leonov A O and Mostovoy M 2015 *Nat. Commun.* **6** 8275
[35] Batista C D, Lin S Z, Hayami S and Kamiya Y 2016 *Rep. Prog. Phys.* **79** 084504
[36] Hayami S, Ozawa R and Motome Y 2017 *Phys. Rev. B* **95** 224424
[37] Wang Q, Sun S S, Zhang X, Pang F and Lei H C 2016 *Phys. Rev. B* **94** 075135
[38] Ye L, Kang M, Liu J, Von Cube F, Wicker C R, Suzuki T, Jozwiak C, Bostwick A, Rotenberg E, Bell D C, Fu L, Comin R and Checkelsky J G 2018 *Nature* **555** 638
[39] Lin Z Y, Choi J H, Zhang Q, Qin W, Yi S, Wang P D, Li L, Wang Y F, Zhang H, Sun Z, Wei L M, Zhang S B, Guo T F, Lu Q Y, Cho J H, Zeng C G and Zhang Z Y 2018 *Phys. Rev. Lett.* **121** 096401
[40] Hou Z, Ren W, Ding B, Xu G, Wang Y, Yang B, Zhang Q, Zhang Y, Liu E, Xu F, Wang W, Wu G, Zhang X, Shen B and Zhang Z 2017 *Adv. Mater.* **29** 1701144
[41] Hou Z, Zhang Q, Xu G, Gong C, Ding B, Wang Y, Li H, Liu E, Xu F, Zhang H, Yao Y, Wu G, Zhang X X and Wang W 2018 *Nano Lett.* **18** 1274
[42] Fenner L A, Dee A A and Wills A S 2009 *J. Phys.: Condens. Matter* **21** 452202
[43] Malaman B, Fruchart D and Caër G L 1978 *J. Phys. F* **8** 2389
[44] Caër G L, Malaman B and Roques B 1978 *J. Phys. F* **8** 323
[45] Kida T, Fenner L A, Dee A A, Terasaki I, Hagiwara M and Wills A S 2011 *J. Phys.: Condens. Matter* **23** 112205
[46] Nagaosa N, Sinova J, Onoda S, MacDonald A H and Ong N P 2010 *Rev. Mod. Phys.* **82** 1539
[47] Wang Q, Xu Y F, Lou R, Liu Z H, Li M, Huang Y B, Shen D W, Weng H M, Wang S C and Lei H C 2018 *Nat. Commun.* **9** 3681